NANO LETTERS

Letter

pubs.acs.org/NanoLett

Atomically Thin Heterostructures Based on Single-Layer Tungsten Diselenide and Graphene

Yu-Chuan Lin,[†] Chih-Yuan S. Chang,[‡] Ram Krishna Ghosh,[§] Jie Li,[§] Hui Zhu,[∥] Rafik Addou,[∥] Bogdan Diaconescu,[⊥] Taisuke Ohta,[⊥] Xin Peng,[∥] Ning Lu,[∥] Moon J. Kim,[∥] Jeremy T. Robinson,[▽] Robert M Wallace,[∥] Theresa S. Mayer,[§] Suman Datta,[§] Lain-Jong Li,*[,‡,#] and Joshua A. Robinson*[,†]

[†]Department of Materials Science and Engineering and Center for 2-Dimensional and Layered Materials, The Pennsylvania State University, University Park, Pennsylvania 16802, United States

[‡]Institute of Atomic and Molecular Sciences, Academia Sinica, Taipei 10617, Taiwan

[§]Department of Electrical Engineering, The Pennsylvania State University, University Park, Pennsylvania 16802, United States

[∥]Department of Materials Science and Engineering, The University of Texas at Dallas, Richardson, Texas 75080 United States

[⊥]Sandia National Laboratories, Albuquerque, New Mexico 87185, Untied States

[▽]Naval Research Laboratory, Washington, DC 20375, United States

[#]Physical Science and Engineering Division, King Abdullah University of Science and Technology, Thuwal 23955-6900, Saudi Arabia

Supporting Information

ABSTRACT: Heterogeneous engineering of two-dimensional layered materials, including metallic graphene and semiconducting transition metal dichalcogenides, presents an exciting opportunity to produce highly tunable electronic and optoelectronic systems. In order to engineer pristine layers and their interfaces, epitaxial growth of such heterostructures is required. We report the direct growth of crystalline, monolayer tungsten diselenide (WSe_2) on epitaxial graphene (EG) grown from silicon carbide. Raman spectroscopy, photoluminescence, and scanning tunneling microscopy confirm high-quality WSe_2 monolayers, whereas transmission electron microscopy shows an atomically sharp interface, and low energy electron diffraction confirms near perfect orientation between WSe_2 and EG. Vertical transport measurements across the WSe_2/EG heterostructure provides evidence that an additional barrier to carrier transport beyond the expected WSe_2/EG band offset exists due to the interlayer gap, which is supported by theoretical local density of states (LDOS) calculations using self-consistent density functional theory (DFT) and nonequilibrium Green's function (NEGF).

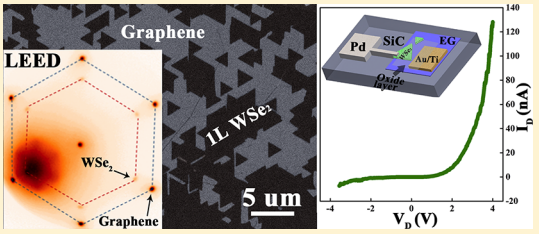

KEYWORDS: *direct growth, heterostructures, graphene, tungsten diselenide (WSe_2), LEED/LEEM, electron tunneling, conductive AFM*

Analogous to the evolution of graphene research,[1] the scientific community is at the initial stage of forming and characterizing van der Waals (vdW) heterostructures, where samples are produced mainly through mechanical exfoliation and manual transfer stacking.[2,3] Unlike isolated monolayer samples, the transfer stacking process can lead to uncontrollable interface contamination that in turn results in reduced device performance.[4] Therefore, developing synthetic techniques to form such heterostructures is critical for engineering pristine layers and junction interfaces. Efforts toward this end include the vertical integration of two-dimensional (2D) materials such as molybdenum disulfide (MoS_2) and hexagonal boron nitride (hBN) on epitaxial graphene (EG).[5] Similarly, chemical vapor deposited (CVD) graphene grown on Cu foils has been utilized as "universal template" for the synthesis of vertical hBN or MoS_2,[6,7] or lateral (in-plane) hBN/graphene systems.[8] In either case, monolayer growth control is essential to exploit phenomena such as the direct-gap crossover in transition metal dichalcogenides (TMDs)[9] or interlayer coupling that can hybridize the electronic structure of stacked monolayers.[10] In this report, we demonstrate direct growth of high-quality WSe_2 monolayers on epitaxial graphene (EG) and provide evidence that this heterosystem exhibits pristine interfaces, high-quality structural, chemical, and optical properties, and significant tunnel resistances due to the WSe_2/EG interlayer gap.

Epitaxial graphene grown from silicon carbide (SiC)[11,12] is an ideal platform to investigate the nucleation and growth of vdW heterostructures. In particular, EG on SiC eliminates the need for postgrowth transfer required for chemical vapor deposited graphene and therefore provides a chemically pristine starting surface. Epitaxial graphene is synthesized by Si sublimation from the (0001) plane (Si face) of semi-insulating on-axis 6H-

Received: August 15, 2014
Revised: October 23, 2014
Published: November 10, 2014

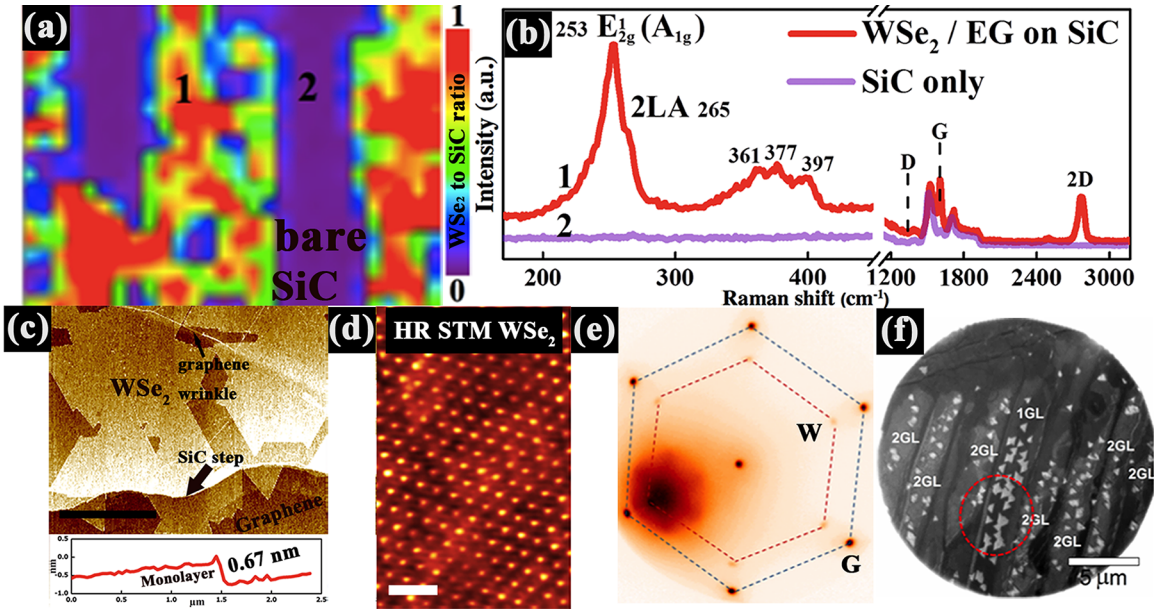

Figure 1. Raman spectroscopy (λ = 488 nm) reveals that (a, b) WSe_2 monolayers selectively growing on EG and not on bare SiC. Atomic force microscopy (c) confirms WSe_2 domains are 3−5 μm along an edge, and with coverage of >50% after a 30 min growth (scale bar is 5 μm). High resolution STM (d) also demonstrates a high quality atomic structure (0.35 V, 1.5 nA, scale bar is 1 nm) and confirms the hexagonal pattern characteristic of 2H-WSe_2. LEED patterns (e) of the WSe_2 (W) on EG (G) confirms a close azimuthal alignment of WSe_2 and EG lattices, and LEEM imaging (f) illustrates the impact of graphene layer thickness on WSe_2 domain formation, where 1−2 layers of EG yield ideal surfaces for large domain WSe_2.

SiC (II−VI, Inc.) at 1725 °C, 200 Torr, in ultrahigh purity argon (Ar).[5] The optimized synthesis leads to uniform step bunching and atomically flat graphene surfaces on the SiC (0001) plane (see Supporting Information, Figure S1a, b). Tungsten diselenide (WSe_2) layers were subsequently synthesized on EG via vapor phase transport of tungsten trioxide (WO_3) in the presence of Ar/H_2 and selenium vapor at 925−1000 °C.[13]

Epitaxial graphene plays an important role in the nucleation and growth of WSe_2. Raman mapping (Figure 1a) shows that WSe_2 (A_{1g}/E_{2g} peak ~250 cm^{-1}) monolayers only grow where graphene (1580 and 2700 cm^{-1}) is present and not on regions of bare SiC (Figure 1b). The selective growth of WSe_2 on graphene indicates that a notable difference in surface energy and sticking coefficient exist between SiC and EG, and that EG provides a more favorable surface for nucleation and growth of the WSe_2. Growth selectivity that depends on surface energy or sticking coefficient may be exploited for templated growth of van der Waals heterostructures and requires subsequent theoretical consideration to elucidate the fundamental physics of growth selectivity in this system. Beyond selectivity, atomic force microscopy (AFM) reveals that the growth rate of WSe_2 is slow (see Supporting Information), with monolayer coverage remaining <75% after a 60 min exposure to the WSe_2 precursors (see Supporting Information). As a result, WSe_2 domain size is highly dependent on synthesis temperature, with the largest domains being achieved at 1000 °C (Figure 1c). The height of individual WSe_2 domains measures 0.71 nm (Figure 1c), and atomic arrangement (Figure 1d) matches that of 2H-WSe_2,[14] in good agreement with previous reports on CVD WSe_2.[13]

Morphological features in the EG (such as wrinkles, SiC step edges, and other surface imperfections) appear to directly influence WSe_2 monolayer development by acting as a barrier to further lateral growth, or by modifying the registry of the WSe_2 layers on epitaxial graphene. A qualitative assessment of the WSe_2 in-plane orientation via AFM suggests a narrow distribution with >80% of the triangles aligned to the underlying graphene (see Supporting Information). Using low energy electron microscopy/diffraction (LEEM/LEED) we are able to quantify the in-plane crystalline orientation of WSe_2 monolayers on EG (Figure 1c,e). Unlike the diffuse LEED patterns of monolayer MoS_2 or $MoSe_2$ on SiO_2,[15,16] the LEED spots of monolayer WSe_2/EG are sharp (Figure 1e), resembling that found for twisted bilayer graphene on SiC.[17] The red and the blue hexagons in Figure 1e illustrate the diffraction spots for WSe_2 and EG, respectively. The larger WSe_2 lattice constant (3.28 Å)[18] as compared to graphene (2.46 Å) means the WSe_2 diffraction spots will be closer to the specular beam (central spot), where both crystals display hexagonal symmetry. The ratio of their lattice constants matches the ratio of the hexagons' sizes (~1.3, extracted from our experiment) and corresponds to a 23% lattice mismatch. Acquiring diffraction from multiple WSe_2 islands simultaneously (Figure 1e) confirms that WSe_2 is not randomly orientated but maintains an in-plane orientation aligned to the underlying graphene layer. A quantitative analysis of the LEED patterns show a less than ±5° variation of the relative orientation of the WSe_2 islands with respect to the EG layer (not shown). The azimuthal alignment between WSe_2 and EG, despite a significant lattice mismatch, suggests that growth proceeds via van der Waals epitaxy.[19,20] Such epitaxy leads to a long-range commensurate structure, where every third W atom in WSe_2 matches every fourth C atom graphene forming a heterostructure unit cell with a lattice constant equal to 9.84 Å (3 and 4 times the WSe_2 and graphene lattice constants, respectively).

It is well known that the electron reflectivity spectra obtained through LEEM measurements (LEEM-IV) can provide the "fingerprint" of the EG thickness.[21,22] By combining the information on EG's thickness together with WSe_2 island

dx.doi.org/10.1021/nl503144a | Nano Lett. 2014, 14, 6936−6941

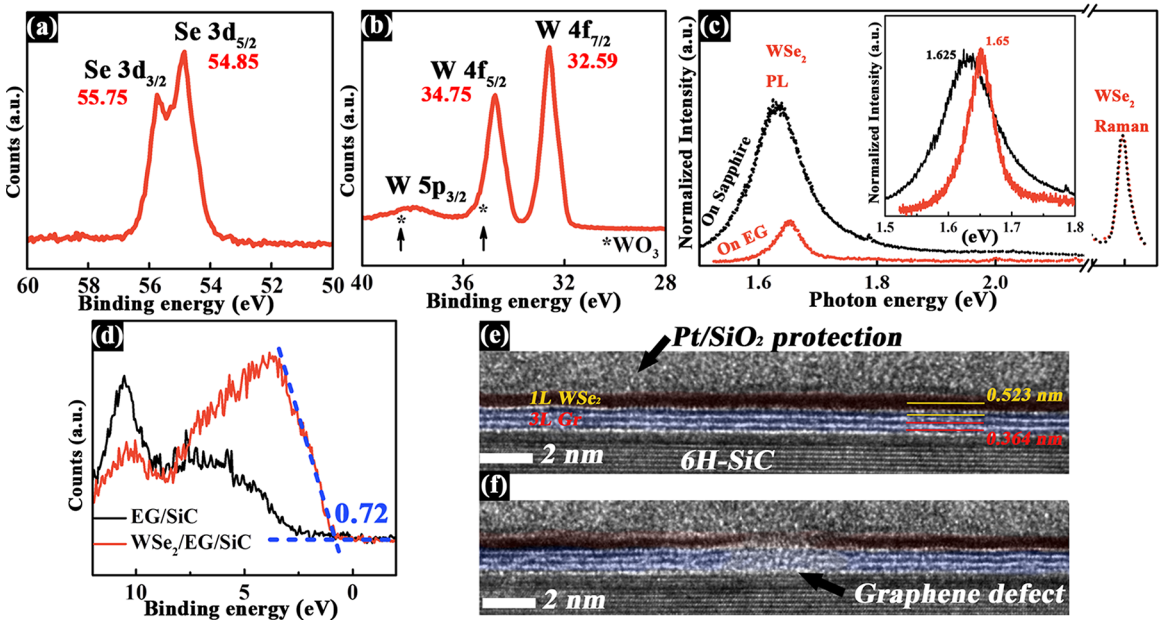

Figure 2. X-ray photoelectron spectroscopy (a,b,c) of the WSe_2/EG heterostructure reveals that the only bonding within the heterostructure is tungsten to selenium. The position of the individual binding energies of W 4f (a) and Se 3d (b) are consistent with p-type doping of the WSe_2.[14] This is confirmed via (d) valence band maxima (VBM) measurements of the WSe_2/EG/SiC system, which is measured to be 0.72 eV below the Fermi-level. The doping of WSe_2 from graphene, as well as the proximity of WSe_2 to graphene leads to significant modifications to the photoluminescence (c) of monolayer WSe_2/EG compared to WSe_2/sapphire. Transmission electron microscopy (e,f) demonstrates that pristine interlayer gaps are possible when the underlying EG is defect-free (e); however, defects in the graphene are translated to the WSe_2 overlayers very effectively (f), resulting in a degraded heterostructure.

density and size, we observe a distinct correlation: The SiC terraces terminated with 1−2 layer EG (confirmed by LEEM I−V) have a higher density of larger WSe_2 islands compared with terraces with more than five layers, which have virtually no WSe_2 islands (Figure 1e and Supporting Information). The triangles in Figure 1e are WSe_2 islands, and the surrounding EG has a darker gray contrast. The terrace located in the middle of the image has, on average, larger WSe_2 islands and higher density. Electron reflectivity spectra reveals this particular terrace is terminated with a monolayer of EG, whereas the neighboring terraces have bilayer EG. We also note that there are virtually no WSe_2 islands located on the narrowest terraces or at step bunches. LEEM-IV confirms these "narrow" terraces are covered by many-layer EG (typically more than five layers). We attribute this this selective growth to the fact that both the sticking coefficient and chemical potential of graphene is sensitive to thickness variation,[5] which likely results in the observed selectivity of WSe_2 on single to few-layer graphene. As a result, one must take care to control the graphene layer thickness to 1−2 layers because the surface properties and chemical reactivity of many-layer graphene layers precludes the formation of large WSe_2 domains, similar to that found for synthesis on graphite.[23]

Direct growth of WSe_2 on EG enables high-quality measurements of the chemical, optical, and structural properties of the heterostructure layers and interfaces. X-ray photoelectron spectroscopy (XPS) confirms there is no measurable reaction between graphene and WSe_2 (Figure 2a, b), and the integrals of high resolution spectra of the Se 3d and W 4f peaks leads an estimated Se:W ratio of approximately 2:1. Recent reports of core-level energies of monolayer WSe_2 on an insulating sapphire substrate using nonmonochromatic Mg Kα X-rays (W $4f_{7/2}$ and W $4f_{5/2}$ peaks are at 32.8 and 35.0 eV, respectively; Se $3d_{5/2}$ and $3d_{3/2}$ peaks are at 55.0 and 55.9 eV, respectively) are noted in the Supporting Information, Table S1.[13] Additionally, the study of bulk, exfoliated p-type WSe_2 with monochromatic Al Kα_1 X-rays indicates that the peaks are shifted to lower values by approximately 0.1 eV.[14] Under identical analysis conditions and parameters to that employed in ref 14, we find here that the monolayer WSe_2/EG exhibits a similar binding energies to exfoliated bulk WSe_2. Based on the bulk WSe_2 core level measurements indicating p-type doping,[14] the WSe_2 monolayers in this work are therefore representative of p-type WSe_2 interfacing with graphene. We also note that a shift in binding energy toward lower energies is consistent with a lower electron density in WSe_2/EG. In other words, EG withdraws electrons from WSe_2 monolayer, leading to p-doped behavior in the WSe_2 layer.[14] This is further confirmed via direct measurements of the occupied valence energy states by XPS, showing that the Fermi level is positioned at 0.72 eV, which is 0.11 eV lower than the midgap energy level in 1 L WSe_2 (0.83 eV). Similar shifts have been reported for other thin films on graphene recently.[24]

To further understand the impact of the underlying EG on the WSe_2 optoelectronic properties, we compare the photoluminescence (PL) spectra of WSe_2 grown on insulating sapphire formed under the same growth conditions (Figure 2d). From this comparison, three features are observed: (i) the PL intensity of WSe_2/EG is quenched by a factor of 3; (ii) the PL peak position of WSe_2/EG is up-shifted by 35 meV (from 1.625 eV on sapphire to 1.66 eV on EG); and (iii) the full width of half-maximum (fwhm) of the WSe_2 PL peak on EG is narrower than WSe_2-on-sapphire (38 meV versus 80 meV). Because the WSe_2 crystalline quality is known to be high on EG (based on LEED, STM, and Raman, Figure 1), the PL quenching is likely a result of photogenerated charge carriers transferring from WSe_2 to EG.[25,26] Zhang et al.[25] proposed the observed quenching in MoS_2/Gr is due to the exciton splitting

dx.doi.org/10.1021/nl503144a | Nano Lett. 2014, 14, 6936−6941

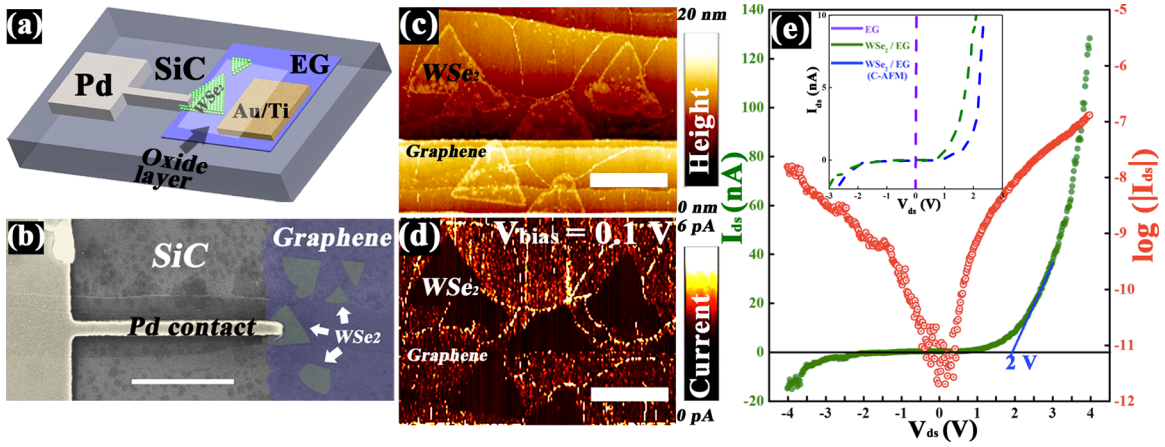

Figure 3. Nanoscale current−voltage characterization indicates that the interlayer gap plays a strong role in vertical transport resistance. The WSe_2/EG diode structure (a,b) consists of a Pd contact to WSe_2, Ti/Au contact to EG, and an oxide overlayer to passivate the WSe_2 surface. The device performance was compared to conductive AFM (platinum tip) as a means to identify how nanoscale transport impacts mesoscale transport in the device structure. Atomic force microscopy indicates that the topography (c) is closely correlated with measure tunneling current (d) between the AFM tip and EG. The measured current versus voltage (I–V) curves from WSe_2/EG diodes and bare EG (e) and C-AFM measurement on WSe_2/EG (e, inset) confirm a large barrier to transport through the heterostructure as well as ~10^5 on/off ratio and turn-on voltage of ~2 V. (b, c, and d scale bar: 1 μm).

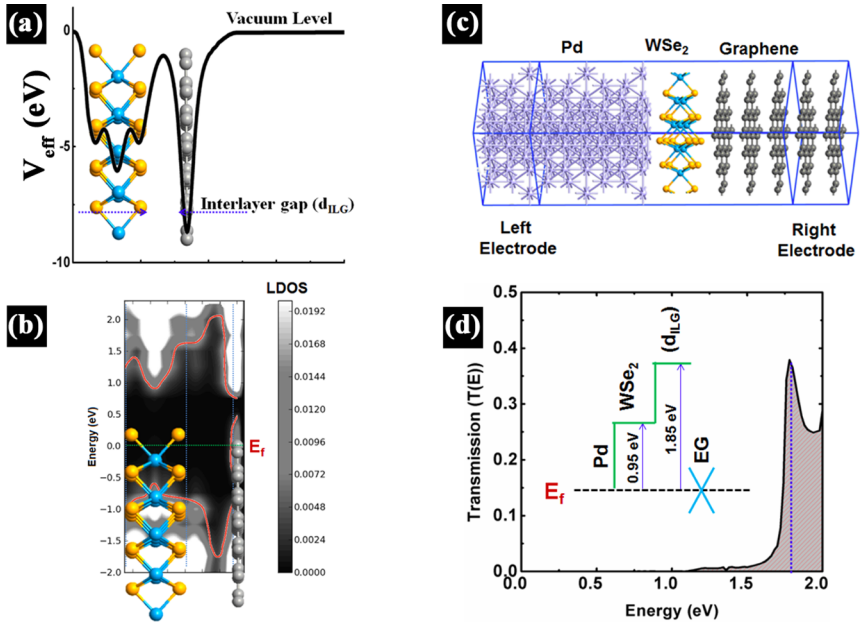

Figure 4. The effective potential profile of a pristine WSe_2/EG heterostructure supercell (a) calculated by density functional theory (DFT) along the out of plane direction demonstrates that a significant finite barrier to electron transport can exist as a result of the inter-layer gap (d_{ILG}). To correlate the potential barrier with a transport barrier, a two terminal device Pd-WSe_2-EG (b) was modeled, and the corresponding local density of states (c) was extracted for the monolayer WSe_2 and the first layer of EG. Finally, the energy resolved transmission spectrum (d) of the Pd-WSe_2-EG demonstrates that vertical transport occurs due to thermal excitation over the inter-layer barrier when the bias is > 1.8 V. The inset shows a schematic of different theoretical barrier heights with respect to the Fermi level in this device.

by the built-in electrical field between 1L CVD graphene and 1L CVD MoS_2. Additionally, Shim et al.[26] observed quenching in $MoSe_2$/graphene heterostructures due to a fast nonradiative recombination process. It is likely that the quenching process for WSe_2/EG observed here is similar in nature. The second feature (red shift of PL peak) could be the result of strain, doping, or defects.[25−28] Our earlier measurements (LEED, STM, and PL) rule out defects and strain as a primary source, and we do find measurable doping of WSe_2 as a result of the EG underlayer (based on XPS). Doping is known to shift PL signatures in MoS_2,[27] which we attribute to the measured PL shift observed in this work. Finally, the PL response of WSe_2/Al_2O_3 (Figure 2c) versus WSe_2/EG here is very similar to a recent report comparing in MoS_2/SiO_2 versus MoS_2/EG and MoS_2/hBN.[28] The narrower peak width suggests that the interface between the WSe_2 and EG is pristine, with no dangling bonds contributing to interface roughness or surface optical phonon scattering.

Cross-sectional TEM confirms the underlying graphene morphology directly influences the nucleation, growth, and structural quality of the WSe_2 overlayer. Where pristine graphene is present, the WSe_2 overlayer is crystalline, with no

dx.doi.org/10.1021/nl503144a | Nano Lett. 2014, 14, 6936−6941

observable defects (Figure 2e). Additionally, the EG interlayer distance is measured to be 3.64 Å (typical for EG/SiC),[29] whereas the WSe_2/EG layer spacing is measured at 5.23 Å, with a WSe_2 thickness of 6.45 Å (see Supporting Information).[18] In regions where graphene is defective, we observe structural disorder in the WSe_2 overlayer (Figure 2f). We note that unlike the MoS_2 grown on EG,[5] in which the SiC $(1\bar{1}0n)$ step edges and EG wrinkles serve as nucleation sites for MoS_2 growth, the WSe_2 abruptly stops at the edge of the $(1\bar{1}0n)$ plane, preferring to grow only on EG synthesized on the SiC (0001) plane. We also point out that WSe_2 is sensitive to electron-beam damage during TEM imaging and it is not stable under high-energy electrons (also seen in LEEM at high electron beam intensity).

Vertical diode structures (Figure 3a,b) and conductive atomic force microscopy (C-AFM; Figure 3c,d) provide a direct means to probe the nanoscale electrical properties of WSe_2/graphene heterostructures. Comparing AFM surface topography and conductivity acquired at V_{bias} = 0.1 V (Figure 3c and d) shows that a barrier to transport exists in the heterojunction regions. The mapping also reveals that the WSe_2 is uniformly resistive and that low resistance contact is possible on the graphene layer, with EG wrinkles and SiC step edges exhibiting enhanced conduction through the AFM tip. Both of the current−voltage (I−V) measurements in C-AFM, and on the diode structures confirm the presence of a tunnel barrier to vertical transport with turn-on occurring at > ± 1.8 V (Figure 3e and inset). To understand the physical mechanism behind the large barrier to transport vertically through the WSe_2 structure, we have investigated the WSe_2/EG heterostructure (Figure 4) using the density functional theory (DFT) (for details see Supporting Information).

Illustrated by the DFT effective potential profile (Figure 4a and Supporting Information Figure S5), the WSe_2 and graphene are weakly bonded by the van der Waals interaction, and the resulting interlayer gap, d_{ILG}, forms a finite potential barrier between them. To identify whether this effective potential profile leads to a true transport barrier, we have performed self-consistent nonequilibrium Green's function (NEGF) transport calculation coupled with DFT, for the Pd/WSe_2/EG vertical structure (Figure 4b). Figure 4c illustrates the spatially resolved local density of states (LDOS) under zero bias. It shows that, within the interlayer gap, d_{ILG}, there are no LDOS contributing to transport. Further, the projected contour line (Figure 4c) of LDOS that delineates the boundary between the negligible (close to zero) LDOS and the finite (0.02) LDOS values provides a quantitative estimate of the transport barrier height arising from the interlayer gap. We estimate this additional barrier to be 1.85 eV above the Fermi level (Figure 4d and inset). Although this model utilizes intrinsic WSe_2 with pristine contacts, it highlights that the gap between the layers plays a critical role in the determination of the turn-on voltage of the layer stack.

The interlayer gap barrier to transport persists up to a bias of 1.80 V (Figure 4d), acting like a thermionic barrier, as evidenced by no appearance of LDOS, agreeing well with experimental measurements showing device turn-on at ∼1.8−2 V. The interlayer gap barrier starts to collapse at a bias beyond 1.85 V, where LDOS appears and contributes to the transport (see Figure 4d). We find theoretically that the barrier due to the interlayer gap depends upon (a) the interlayer gap thickness, d_{ILG}, and (b) the Coulombic interaction among the different atoms of the constituent layers. With the decrease in the interlayer gap, the interaction increases, which reduces the barrier height. For instance, in our system, we observe that the Pd/WSe_2 interlayer gap distance of 2.98 Å is lower than that of the WSe_2/EG 3.53 Å. Hence, the Pd/WSe_2 interlayer barrier height is significantly less than that of WSe_2/EG (see Supporting Information Figure S6). Thus, the barrier arising from the interlayer gap at the WSe_2/EG interface dominates the electronic transport. It is to be noted that our calculations also shows existence of the conventional Schottky barrier of 0.95 eV between the Pd electrode and the monolayer WSe_2.[30]

In conclusion, we demonstrate a synthetic route to forming WSe_2/epitaxial graphene heterostructures via van der Waals epitaxy. Even though the lattice mismatch between WSe_2 and graphene is shown to be 23%, the heterostructure is commensurate at every third W and fourth C atom, indicating the potential to grow single-crystal heterostructures over large areas. Additionally, we provide evidence that the structural, chemical, and optical properties of the WSe_2 grown on graphene match or exceed that of mechanically exfoliated WSe_2 films. Finally, WSe_2/EG diode structures and C-AFM indicate that efficient tunneling is possible through the WSe_2 layer to graphene, and the primary source of tunneling resistance occurs at the interlayer gap between the WSe_2 and graphene layer.

■ ASSOCIATED CONTENT

Supporting Information

Synthesis, device fabrication, and modeling procedures. AFM, STM, PL, and Raman of epitaxial graphene and WSe_2/graphene. This material is available free of charge via the Internet at http://pubs.acs.org.

■ AUTHOR INFORMATION

Corresponding Authors

*E-mail: lance.li@kaust.edu.sa.
*E-mail: jrobinson@psu.edu.

Notes

The authors declare no competing financial interest.

■ ACKNOWLEDGMENTS

The work at Penn State and UT Dallas was supported by the Center for Low Energy Systems Technology (LEAST), one of six centers supported by the STARnet phase of the Focus Center Research Program (FCRP), a Semiconductor Research Corporation (SRC) program sponsored by MARCO and DARPA. Work at UT-Dallas was also supported by the Southwest Academy on Nanoelectronics (SWAN) a SRC center sponsored by the Nanoelectronics Research Initiative and NIST. Device fabrication was supported by the Pennsylvania State University Materials Research Institute Nanofabrication Lab and the National Science Foundation Cooperative Agreement No. ECS-0335765. J.T.R. acknowledges support by NRL Base Programs through the Office of Naval Research. The work at SNL was supported by the US DOE Office of Basic Energy Sciences (BES), Division of Materials Science and Engineering and by Sandia LDRD. Sandia National Laboratories is a multiprogram laboratory managed and operated by Sandia Corporation, a wholly owned subsidiary of Lockheed Martin Corporation, for the U.S. Department of Energy's National Nuclear Security Administration under contract DE-AC04-94AL85000. L.J.L. acknowledges the support from Academia Sinica Taiwan, KAUST Saudi Arabia, and US AOARD-134137. Support for the WiteC

Raman system, Bruker Dimension AFM, and nanofabrication facilities was provided by the National Nanotechnology Infrastructure Net- work at Penn State.

REFERENCES

(1) Geim, A. K.; Grigorieva, I. V. *Nature* **2013**, *499*, 419−425.
(2) Britnell, L.; Gorbachev, R. V.; Jalil, R.; Belle, B. D.; Schedin, F.; Mishchenko, A.; Georgiou, T.; Katsnelson, M. I.; Eaves, L.; Morozov, S. V.; Peres, N. M. R.; Leist, J.; Geim, A. K.; Novoselov, K. S.; Ponomarenko, L. A. *Science* **2012**, *335*, 947−950.
(3) Lee, C.-H.; Lee, G.-H.; van der Zande, A. M.; Chen, W.; Li, Y.; Han, M.; Cui, X.; Arefe, G.; Nuckolls, C.; Heinz, T. F.; Guo, J.; Hone, J.; Kim, P. *Nat. Nanotechnol.* **2014**, *9*, 676−681.
(4) Haigh, S. J.; Gholinia, A.; Jalil, R.; Romani, S.; Britnell, L.; Elias, D. C.; Novoselov, K. S.; Ponomarenko, L. A.; Geim, A. K.; Gorbachev, R. *Nat. Mater.* **2012**, *11*, 764−767.
(5) Lin, Y.-C.; Lu, N.; Perea-Lopez, N.; Li, J.; Lin, Z.; Peng, X.; Lee, C. H.; Sun, C.; Calderin, L.; Browning, P. N.; Bresnehan, M. S.; Kim, M. J.; Mayer, T. S.; Terrones, M.; Robinson, J. A. *ACS Nano* **2014**, *8*, 3715−3723.
(6) Liu, Z.; Song, L.; Zhao, S.; Huang, J.; Ma, L.; Zhang, J.; Lou, J.; Ajayan, P. M. *Nano Lett.* **2011**, *11*, 2032−2037.
(7) Shi, Y.; Zhou, W.; Lu, A.-Y.; Fang, W.; Lee, Y.-H.; Hsu, A. L.; Kim, S. M.; Kim, K. K.; Yang, H. Y.; Li, L.-J.; Idrobo, J.-C.; Kong, J. *Nano Lett.* **2012**, *12*, 2784−2791.
(8) Levendorf, M. P.; Kim, C.-J.; Brown, L.; Huang, P. Y.; Havener, R. W.; Muller, D. A.; Park, J. *Nature* **2012**, *488*, 627−632.
(9) Ohta, T.; Robinson, J. T.; Feibelman, P. J.; Bostwick, A.; Rotenberg, E.; Beechem, T. E. *Phys. Rev. Lett.* **2012**, *109*, 186807.
(10) Robinson, J. T.; Schmucker, S. W.; Diaconescu, C. B.; Long, J. P.; Culbertson, J. C.; Ohta, T.; Friedman, A. L.; Beechem, T. E. *ACS Nano* **2013**, *7*, 637−644.
(11) De Heer, W. A.; Berger, C.; Wu, X.; First, P. N.; Conrad, E. H.; Li, X.; Li, T.; Sprinkle, M.; Hass, J.; Sadowski, M. L.; Potemski, M.; Martinez, G. *Solid State Commun.* **2007**, *143*, 92−100.
(12) Robinson, J.; Weng, X.; Trumbull, K.; Cavalero, R.; Wetherington, M.; Frantz, E.; Labella, M.; Hughes, Z.; Fanton, M.; Snyder, D. *ACS Nano* **2010**, *4*, 153−158.
(13) Huang, J.-K.; Pu, J.; Hsu, C.-L.; Chiu, M.-H.; Juang, Z.-Y.; Chang, Y.-H.; Chang, W.-H.; Iwasa, Y.; Takenobu, T.; Li, L.-J. *ACS Nano* **2014**, *8*, 923−930.
(14) McDonnell, S.; Azcatl, A.; Addou, R.; Gong, C.; Battaglia, C.; Chuang, S.; Cho, K.; Javey, A.; Wallace, R. M. *ACS Nano* **2014**, *8*, 6265−6272.
(15) Yeh, P.-C.; Jin, W.; Zaki, N.; Zhang, D.; Sadowski, J. T.; Al-Mahboob, A.; van der Zande, A. M.; Chenet, D. A.; Dadap, J. I.; Herman, I. P.; Sutter, P.; Hone, J.; Osgood, R. M. *Phys. Rev. B* **2014**, *89*, 155408.
(16) Zhang, Y.; Chang, T.-R.; Zhou, B.; Cui, Y.-T.; Yan, H.; Liu, Z.; Schmitt, F.; Lee, J.; Moore, R.; Chen, Y.; Lin, H.; Jeng, H.-T.; Mo, S.-K.; Hussain, Z.; Bansil, A.; Shen, Z.-X. *Nat. Nanotechnol.* **2014**, *9*, 111−115.
(17) Ohta, T.; Beechem, T. E.; Robinson, J. T.; Kellogg, G. L. *Phys. Rev. B* **2012**, *85*, 075415.
(18) Wilson, J. A.; Yoffe, A. D. *Adv. Phys.* **1969**, *18*, 193−335.
(19) Koma, A. *Thin Solid Films* **1992**, *216*, 72−76.
(20) Ji, Q.; Zhang, Y. Y.; Gao, T.; Ma, D.; Liu, M.; Chen, Y.; Qiao, X.; Tan, P.-H. H.; Kan, M.; Feng, J.; Sun, Q.; Liu, Z. *Nano Lett.* **2013**, *13*, 3870−3877.
(21) Hibino, H.; Kageshima, H.; Maeda, F.; Nagase, M.; Kobayashi, Y.; Yamaguchi, H. *Phys. Rev. B: Condens. Matter Mater. Phys.* **2008**, *78*, 245403.
(22) Riedl, C.; Coletti, C.; Iwasaki, T.; Zakharov, A. A.; Starke, U. *Phys. Rev. Lett.* **2009**, *103*, 246804.
(23) Zhang, C.; Johnson, A.; Hsu, C.-L.; Li, L.-J.; Shih, C.-K. *Nano Lett.* **2014**, *14*, 2443−2447.
(24) Coy Diaz, H.; Addou, R.; Batzill, M. *Nanoscale* **2014**, *6*, 1071−1078.
(25) Zhang, W.; Chuu, C.-P.; Huang, J.-K.; Chen, C.-H.; Tsai, M.-L.; Chang, Y.-H.; Liang, C.-T.; Chen, Y.-Z.; Chueh, Y.-L.; He, J.-H.; Chou, M.-Y.; Li, L.-J. *Sci. Rep.* **2014**, *4*, 3826.
(26) Shim, G. W.; Yoo, K.; Seo, S.-B.; Shin, J.; Jung, D. Y.; Kang, I.-S.; Ahn, C. W.; Cho, B. J.; Choi, S.-Y. *ACS Nano* **2014**, *8*, 6655−6662.
(27) Mouri, S.; Miyauchi, Y.; Matsuda, K. *Nano Lett.* **2013**, *13*, 5944−5948.
(28) Buscema, M.; Steele, G. A.; van der Zant, H. S. J.; Castellanos-Gomez, A. *Nano Res.* **2014**, *7*, 561−571.
(29) Weng, X.; Robinson, J. A.; Trumbull, K.; Cavalero, R.; Fanton, M. A.; Snyder, D. *Appl. Phys. Lett.* **2010**, *97*, 201905.
(30) Das, S.; Appenzeller, J. *Appl. Phys. Lett.* **2013**, *103*, 103501.